Asian Journal of Chemistry; Vol. 35, No. 10 (2023), 2498-2508

ASIAN JOURNAL OF CHEMISTRY

https://doi.org/10.14233/ajchem.2023.28190

Quantum Chemical Studies on Structural, Spectral and Frontier Molecular Orbital Analysis of Indometacin in Aqueous Phases

B. YOGESWARI[1,*], S. DEIVANAYAKI[2], A. SAJITHA BANU[3] and E. JAYANTHI[4]

[1]Department of Physics, Sri Eshwar College of Engineering (Autonomous), Coimbatore-641202, India
[2]Department of Physics, Sri Ramakrishna Engineering College (Autonomous), Coimbatore-641022, India
[3]Department of Physics, PSNA College of Engineering and Technology (Autonomous), Dindigul-624622, India
[4]Department of Chemistry, Kongunadu Arts and Science College (Autonomous), Coimbatore-641029, India

*Corresponding author: E-mail: yogeshwari.b@sece.ac.in

Received: 29 June 2023; *Accepted*: 20 August 2023; *Published online*: 28 September 2023; AJC-21403

Density functional theory computations were done by using 6-31G(d) basis set in order to check out the solubility of indometacin in polar and non-polar solvents such as water, ethanol, acetone and diethyl ether, respectively. The quantum chemical parameters of indometacin in gaseous as well as in aqueous phases were calculated. The most stable structure (indometacin in water; IM-W) was found to be more stable with respect to the least stable complex (indometacin in diethyl ether; IM-D) by 3.14 Kcal/mol. The zero-point vibrational energy of indometacin in gas phase was found to be 197.731 Kcal/mol. The fundamental vibrational modes of indometacin were assignment and analyzed at B3LYP/6-31G(d) level of theory. The HOMO–LUMO analysis of indometacin showed that its HOMO is concentrated at its indole ring and LUMO is at its chlorophenyl group. The charge density distribution of indometacin was investigated through the molecular electrostatic potential map.

Keywords: Indometacin, Self-consistent reaction field theory, Vibrational modes, HOMO-LUMO, Molecular electrostatic potential.

INTRODUCTION

Indometacin is considered as an important and most potent non-steroidal anti-inflammatory drug (NSAID) used for the migraine treatment, acute ache, gout, inflammation and signs of arthritis. Indometacin ($C_{19}H_{16}NO_4Cl$) is an indole-acetic acid derivative with the IUPAC name 2-[1-(4-chlorobenzoyl)-5-methoxy-2-methylindol-3-yl] acetic acid [1]. Indometacin is also valuable for treating ankylosing spondylitis that affects the spine joints and found to be useful in bursitis treatment, a treatment for an inflammation of a bursa, specifically in the shoulder joints [2,3]. Indometacin demonstrates good anti-tumor activity against cyclooxygenase 2 (COX-2), an enzyme believed to be present in tumor cells [3]. The indometacin is found to be effective for COVID-19 infection and its efficiency is noted to be somewhat elevated compared to the well-known medicines for instance remdesivir, hydroxyl chloroquine and lopinavir [4]. This demonstrates indometacin's growth prospective against SARS-CoV-2 as an antiviral entity.

Indometacin is currently given orally as well as *via* rectal and intravenous methods. An oral route medication necessitates excellent water solubility as a primary requirement. Simultaneously, the appropriate absorption and bioavailability of active oral medicines, such as indomethacin (0.937 mg/L at 25 ºC), seems to be an essential issue [5]. Due to indometacin's limited solubility in water, local drug concentrations decrease the medicine's therapeutic efficacy and cause tissue ulceration. Most NSAIDs, including indometacin have poor water solubility resulting in meager bioavailability and irregular absorption. Hydrotropes are surface-active compounds soluble in water and can notably influence the solubility of drugs with feeble solubility. Numerous studies have been conducted to investigate the utilization of various hydrotropes in order to enhance the solubility of indometacin [6-10].

Laguna *et al*. [9] used a DFT-molecular modeling investigation to study the copper(II)-indometacin in ethanol and water as a metal-NSAID model. They attempted to present an imperative perceptive method of poorly dissoluble medicines *via*

UV-visible spectrophotometry. Jain [11] used UV, IR and X-ray diffraction methods to study the impact of several hydrotropes such as urea, nicotinamide, resorcinol, *etc*. and analyzed the solubility of indometacin for aqueous injection and concluded that the solubility of indometacin with various hydrotropes at lower and higher concentrations are because of feeble ionic interactions and aggregation of molecules. Qi *et al*. [12] identified freeze-drying as a suitable method to enrich the solubility of indometacin and its self life by using arginine as a hydrotrope.

Surfactants are the surface-active mediators added to a substance to increase its dispersion and wetting by reducing its surface tension. Using spectrophotometric analysis, Yackevich *et al*. [13] determined that indometacin was more soluble in micellar solutions of several dicationic surfactants. The solubility of indometacin was also determined in different solvents such as castor oil and labrafil in the presence of some solubilizing agents and attempted to prepare an eye drop formulation [14]. Shende *et al*. [15] compared the impact of various solubility techniques, such as hydrotropy, solid dispersion and freeze drying, to improve the solubility of indometacin and declared that the solid dispersion was found to be suitable in order to attain the highest solubility of indometacin. Rodríguez-Laguna *et al*. [16] employed UV-visible spectrometry and molecular modeling in DFT methods to explore the therapeutic characteristics of copper-indometacin systems of various concentrations with ethanol and water as hydrotropes. Additionally, it is thought that changes in the solute's physical and chemical properties are the result of interactions between the molecules of the solute and the solvent. Also, information about the modifications in the molecular energies of solutes in various atmospheres provides details about the influence of solvents on their molecular geometry and stability.

This work aims to carry out the density functional calculations in order to check out the solubility of indometacin in polar and non-polar solvents such as water (ε = 78.5), ethanol (ε = 24.852), acetone (ε = 20.493) and diethyl ether (ε = 4.24), respectively. In present study, the optimized indometacin in the gas phase was further investigated in the aqueous environments. The quantum chemical parameters and the vibrational wave numbers of indometacin in gaseous and aqueous phases were analyzed. The molecular electrostatic potential (MEP) map and the highest occupied molecular orbital (HOMO) and lowest unoccupied molecular orbital (LUMO) energy levels of frontier orbitals involved in indometacin in gaseous and aqueous phases have been analyzed.

COMPUTATIONAL METHODS

To begin with, the structure of indometacin was recaptured from the NCBI PubChem database [17]. Becke's three-parameter exact exchange functional (B3) [18] with gradient corrected correlation functional of Lee-Yang-Parr (LYP) [19] of density functional theory (DFT) methods were used to optimize indometacin molecule in both the phases by implementing the 6-31G (d) basis set through Gaussian 09 program [20]. The same method is implemented to investigate the thermo dynamical properties, vibrational wave numbers, MEP map and the HOMO-LUMO energy levels of indometacin in gaseous and aqueous phases. Gaussview program [21] has been utilized to analyze the vibrational wave number assignments of indometacin. The solute-solvent interactions were studied through the self-consistent reaction field theory (SCRF), supported by Tomasi's Polarized Continuum Model (PCM) [22] at B3LYP/6-31G(d) method. Here, the indometacin was placed in the cavity within water (ε = 78.5), ethanol (ε = 24.852), acetone (ε = 20.493) and diethyl ether (ε = 4.24) as solvents.

RESULTS AND DISCUSSION

The structure of optimized indometacin with atom labeling is shown in Fig. 1. The indometacin in gaseous and aqueous phases *viz*. water, ethanol, acetone and diethyl ether are named IM, IM-W, IM-E, IM-A and IM-D, respectively, for convenience. The bond lengths and angles of indometacin in gaseous as well as aqueous phases are presented in Tables 1 and 2, respectively, along with the available previous theoretical values [23].

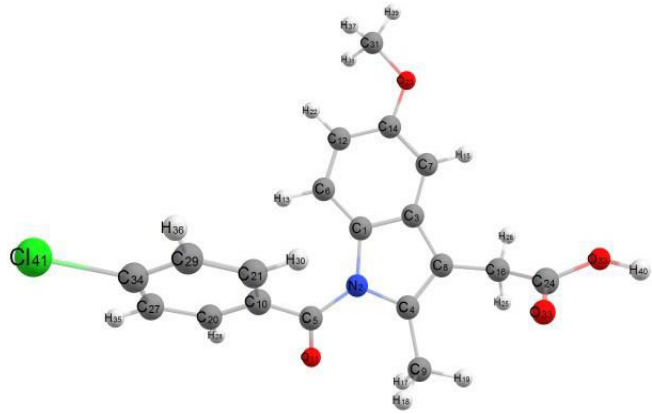

Fig. 1. Optimized structure of indometacin with B3LYP/6-31G(d) level of theory

Fig. 2 presents the comparative graph of indometacin bond lengths with previous theoretical values. Some of the present optimized bond lengths of indometacin are observed to be larger than the previous theoretical results calculated at the DFT/B3LYP 6-31G level. These variations might result from different levels of theory's optimization of geometrical parameters. It is significant to observe that the bond lengths associated with the carboxylic acid group of indometacin predicted by both studies are nearly identical.

The comparative graph of the bond lengths of indometacin in gaseous and aqueous phases is presented in Fig. 3. There are no notable variations in the bond lengths of indometacin between gaseous and aqueous phases, which shows that the geometry of indometacin is less affected by the presence of different aqueous environments. It may be because the solute-solvent interactions are typically much lesser than intramolecular forces, which would not alter the geometry much as it moves from the gas to the solution phases.

The calculated total energy, relative energy and the dipole moments of indometacin in gaseous and aqueous phases computed with B3LYP/6-31G(d) method have been given in Table-3. The results predicted an increase in the order of stability of solvated indometacin aqueous phases as IM-W > IM-E > IM-A

TABLE-1
GAS PHASE, AQUEOUS AND DIFFERENT SOLVENTS MOLECULAR GEOMETRICAL BOND LENGTHS (Å) OF INDOMETACIN CALCULATED AT B3LYP/6-31G(d) LEVEL OF THEORY. FOR LABELING OF ATOMS, REFER TO Fig. 1

Bond length (Å)	Indometacin	Indometacin in aqueous phases			
		Water (ε = 78.5)	Acetone (ε = 20.493)	Ethanol (ε = 24.852)	Diethyl ether (ε = 4.24)
C1-N2	1.416 (1.27)[a]	1.418	1.417	1.417	1.417
C1-C3	1.415 (1.34)[a]	1.413	1.414	1.414	1.414
C1-C6	1.393	1.393	1.393	1.393	1.393
N2-C4	1.415 (1.28)[a]	1.415	1.417	1.417	1.417
N2-C5	1.410 (1.27)[a]	1.407	1.408	1.408	1.408
C3-C7	1.397	1.398	1.397	1.397	1.397
C3-C8	1.445 (1.34)[a]	1.446	1.446	1.446	1.445
C4-C8	1.368 (1.35)[a]	1.373	1.368	1.368	1.368
C4-C9	1.495	1.496	1.496	1.496	1.496
C5-C10	1.495	1.494	1.493	1.493	1.494
C5-O11	1.221	1.222	1.224	1.224	1.223
C6-C12	1.397	1.397	1.397	1.397	1.397
C6-H13	1.083	1.082	1.083	1.083	1.083
C7-C14	1.397	1.398	1.398	1.398	1.397
C7-H15	1.086	1.084	1.086	1.086	1.086
C8-C16	1.499	1.497	1.497	1.497	1.497
C9-H17	1.094	1.098	1.093	1.093	1.093
C9-H18	1.095	1.096	1.096	1.096	1.096
C9-H19	1.092	1.090	1.092	1.092	1.093
C10-C20	1.402	1.403	1.403	1.403	1.402
C10-C21	1.402	1.403	1.403	1.403	1.403
C12-C14	1.408	1.408	1.408	1.408	1.408
C12-H22	1.083	1.085	1.083	1.083	1.083
C14-O23	1.369	1.367	1.369	1.369	1.369
C16-C24	1.524 1.520a	1.523	1.522	1.522	1.523
C16-H25	1.099	1.097	1.096	1.096	1.096
C16-H26	1.094	1.101	1.098	1.098	1.098
C20-C27	1.391	1.388	1.392	1.392	1.392
C20-H28	1.085	1.085	1.085	1.085	1.085
O23-C31	1.417	1.425	1.424	1.424	1.422
C24-O32	1.357 (1.35)[a]	1.355	1.352	1.352	1.354
C24-O33	1.210 (1.21)[a]	1.220	1.213	1.213	1.211
C27-C34	1.396	1.396	1.396	1.396	1.396
C27-H35	1.085	1.085	1.084	1.084	1.084
C29-C34	1.395	1.397	1.395	1.395	1.395
C29-H36	1.085	1.084	1.084	1.084	1.084
C31-H37	1.099	1.098	1.097	1.097	1.097
C31-H38	1.098	1.097	1.097	1.097	1.098
C31-H39	1.092	1.092	1.091	1.091	1.091
O32-H40	0.976 (0.97)[a]	0.979	0.977	0.977	0.976
C34-Cl41	1.755	1.762	1.759	1.759	1.758

[a]From Ref. [23] optimized at DFT/B3LYP 6-31G level of theory.

TABLE-2
GAS PHASE, AQUEOUS AND DIFFERENT SOLVENTS MOLECULAR GEOMETRICAL BOND ANGLES (°) OF INDOMETACIN CALCULATED AT B3LYP/6-31G(d) LEVEL OF THEORY. FOR LABELING OF ATOMS, REFER TO Fig. 1

Bond angle (°)	Indometacin	Indometacin in aqueous phases			
		Water (ε = 78.5)	Acetone (ε = 20.493)	Ethanol (ε = 24.852)	Diethyl ether (ε = 4.24)
N2-C1-C3	107.2	107.3	107.2	107.2	107.2
N2-C1-C6	131.8	131.8	131.8	131.8	131.8
C1-N2-C4	108.2 (109.54)[a]	108.1	108.1	108.1	108.1
C1-N2-C5	127.6	127.4	127.4	127.4	127.4
C3-C1-C6	120.8	120.8	120.8	120.8	120.8
C1-C3-C7	120.1	120.3	120.2	120.2	120.2
C1-C3-C8	107.4	107.6	107.6	107.6	107.5
C1-C6-12	118.6	118.6	118.6	118.6	118.6
C1-C6-13	122.0	121.9	122.1	122.1	122.1
C4-N2-C5	123.7	124.2	124.0	124.0	124.0
N2-C4-C8	109.1	109.2	109.1	109.1	109.1

N2-C4-9	122.4	122.2	122.1	122.1	122.1
N2-C5-10	118.0	117.8	118.0	118.0	118.0
N2-C5-11	121.1	121.1	121.0	121.0	121.1
C7-C3-C8)	132.4	132.1	132.2	132.2	132.2
C3-C7-14)	119.1	119.0	119.0	119.0	119.0
C3-C7-15	122.1	121.9	121.9	121.9	121.9
C3-C8-C4	108.1	107.8	108.0	108.0	108.0
C3-C8-16	125.0	125.1	124.8	124.8	124.7
C8-C4-C9	128.4	128.5	128.7	128.7	128.7
C4-C8-C16	127.0	127.2	127.2	127.2	127.3
C4-C9-H17	112.0	111.7	112.0	112.0	112.0
C4-C9-H18	111.4	111.5	111.4	111.4	111.4
C4-C9-H19	109.4	110.1	109.8	109.8	109.7
C10-C5-O11	120.8	121.0	120.9	120.9	120.8
C5-C10-C20	117.8	118.3	118.1	118.1	118.0
C5-C10-C21	122.6	122.0	122.2	122.2	122.3
C12-C6-H13	119.4	119.5	119.3	119.3	119.3
C6-C12-C14	120.9	120.9	120.9	120.9	120.9
C6-C12-H22	118.5	118.3	118.5	118.5	118.5
C14-C7-H15	118.8	119.1	119.1	119.1	119.1
C7-C14-C12	120.4	120.4	120.4	120.4	120.4
C7-C14-O23	115.6	115.8	115.7	115.7	115.6
C8-C16-C24	114.1	114.0	114.2	114.2	114.2
C8-C16-H25	111.1	111.7	111.7	111.7	111.7
C8-C16-H26	111.0	110.8	110.8	110.8	110.9
H17-C9-H18	106.9	106.8	107.0	107.0	107.0
H17-C9-H19	109.6	108.6	108.8	108.8	108.9
H18-C9-H19	107.4	107.8	107.8	107.8	107.7
C20-C10-C21	119.3	119.3	119.4	119.4	119.4
C10-C20-C27	120.7	120.8	120.7	120.7	120.7
C10-C20-H28	118.9	119.0	119.3	119.3	119.2
C10-C21-C29	120.5	120.6	120.5	120.5	120.5
C10-C21-H30	120.1	120.3	120.2	120.2	120.2
C14-C12-H22	120.6	120.8	120.6	120.6	120.6
C12-C14-O23	124.0	123.8	124.0	124.0	124.0
C14-O23-C31	118.4	118.5	118.4	118.4	118.4
C24-C16-H25	105.9	107.1	107.1	107.1	107.0
C24-C16-H26	108.6	107.5	107.3	107.3	107.4
C16-C24-O32	111.1	110.9	110.7	110.7	110.6
C16-C24-O33	126.1	126.5	126.5	126.5	126.6
H25-C16-H26	105.7	105.3	105.2	105.2	105.2
C27-C20-H28	120.4	120.2	120.0	120.0	120.1
C20-C27-C34	119.0	118.8	118.8	118.8	118.9
C20-C27-H35	120.9	120.9	120.8	120.8	120.8
C29-C21-H30	119.4	119.1	119.3	119.3	119.3
C21-C29-C34	119.1	118.8	119.0	119.0	119.0
C21-C29-H36	120.7	120.8	120.6	120.6	120.6
O23-C31-H37	111.7	111.4	111.5	111.5	111.6
O23-C31-H38	111.7	111.6	111.6	111.6	111.6
O23-C31-H39	105.9	105.7	105.8	105.8	105.9
O32-C24-O33	122.7 (123.94)[a]	122.6	122.9	122.9	122.8
C24-O32-H40	106.0	107.3	107.1	107.2	106.8
C34-C27-H35	120.1	120.3	120.4	120.4	120.3
C27-C34-C29	121.3	121.7	121.6	121.6	121.5
C27-C34-Cl41	119.3	119.2	119.2	119.2	119.2
C34-C29-H36	120.1	120.5	120.4	120.4	120.4
C29-C34-H41	119.3	119.1	119.2	119.2	119.2
H37-C31-H38	109.1	109.3	109.3	109.3	109.2
H37-C31-H39	109.2	109.1	109.3	109.3	109.3
H38-C31-H39	109.2	109.5	109.3	109.3	109.2

[a]From Ref. [23] optimized at DFT/B3LYP 6-31G level of theory.

TABLE-3
TOTAL ENERGY, E (Hartree), RELATIVE ENERGY, ΔE (Kcal/mol), DIPOLE MOMENT, μ_m (debye), THERMAL ENERGIES (TRANSLATIONAL (Q_T), ROTATIONAL (Q_R) AND VIBRATIONAL (Q_V) (Kcal/mol), SPECIFIC HEAT (CV) (Cal/Mol-K), ENTROPY (S) (Cal/Mol-K), ZERO-POINT VIBRATIONAL ENERGY (ZPVE) (Kcal/mol) AND ROTATIONAL CONSTANTS R_A, R_B, R_C (GHz) FOR THE INDOMETACIN IN GASEOUS AND AQUEOUS PHASES (WATER, ACETONE, ETHANOL AND DIETHYL ETHER) CALCULATED AT B3LYP/6-31G(d) LEVEL OF THEORY

Parameters	Indometacin	Indometacin in aqueous phases			
		Water (ε = 78.5)	Acetone (ε = 20.493)	Ethanol (ε = 24.852)	Diethyl ether (ε = 4.24)
-E	1549.521	1549.536	1549.535	1549.5355	1549.531
ΔE	–	9.41	8.79	9.09	6.28
μ_m	2.237	1.981	1.972	1.972	1.919
Q_T	0.889	0.889	0.889	0.889	0.889
Q_R	0.889	0.889	0.889	0.889	0.889
Q_V	210.147	209.840	209.857	209.853	209.933
CV	85.027	85.236	85.222	85.225	85.167
S	165.206	164.861	164.745	164.766	164.620
ZPVE	197.731	197.420	197.441	197.436	197.526
R_A	0.264	0.275	0.275	0.275	0.275
R_B	0.117	0.115	0.115	0.115	0.115
R_C	0.092	0.093	0.093	0.093	0.092

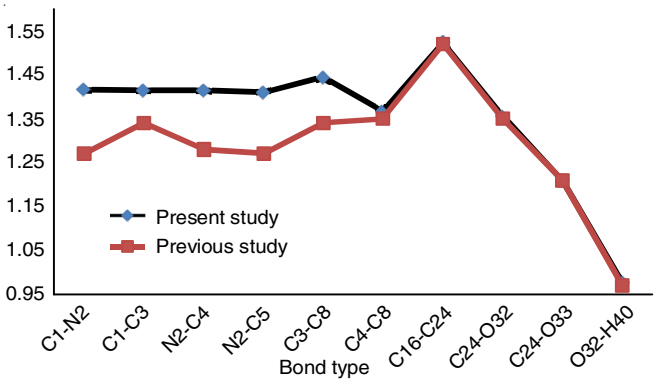

Fig. 2. Comparison of bond lengths with previous theoretical values

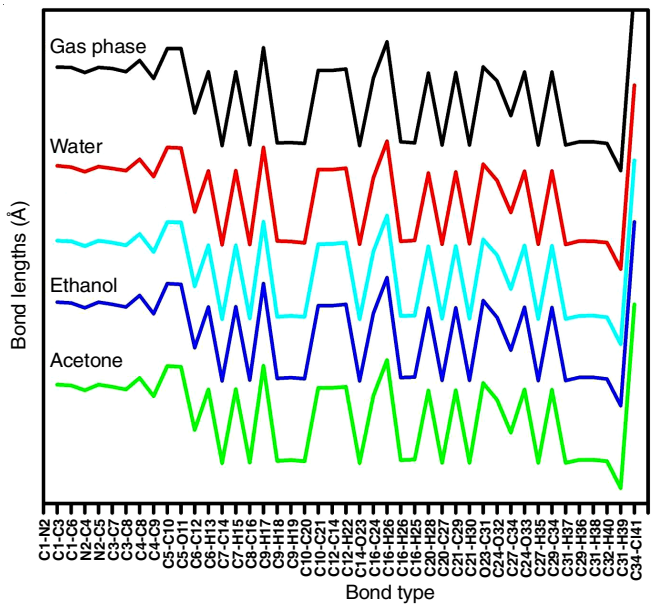

Fig. 3. Comparative graph of the bond lengths of indometacin in gaseous and liquid phases

> IM-D and it is interesting to observe that the stability of solvated indometacin increases with increasing dielectric constants as well as the dipole moments.

The most stable structure IM-W is found to be more stable with respect to the least stable complex IM-D, by 3.14 Kcal/mol. The solvent interaction with indometacin significantly increased its stability which is substantiated by the decrease in energy values of the solvated molecule which is reflected in the form of relative energy values given in Table-3.

A molecule having N atoms has (3N-6) normal modes of vibrations excluding three rotational degrees of freedom [24]. Here, indometacin with 41 atoms shows 117 normal vibrations modes active in infrared and Raman absorptions. The DFT methods are a better option for the accurate prediction of modes of vibrations of polyatomic molecules exceeding 50 [25]. The theoretically calculated infrared frequencies of indometacin calculated with B3LYP/6-31G(d) in gaseous as well as solution phases were presented in Figs. 4 and 5, respectively and the values are presented in Table-4. The Raman spectroscopy and intensities are accepted to be a dependable tool for recognizing and investigating the potential enhancement of anti-inflammatory and new drugs, including indometacin [26].

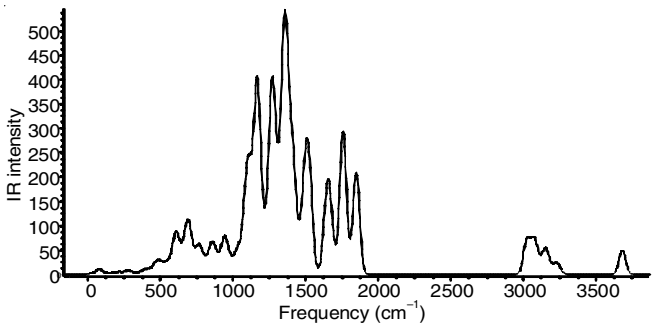

Fig. 4. Recorded IR intensities of indometacin in gas phase

Figs. 6 and 7 present the computed Raman intensities of the title molecule in gas and aqueous phases. Except for a few, the IR intensities of indometacin in its gaseous and aqueous phases are identical. The same trend applies to Raman intensities also. The C-H vibrations are generally observed in the range of 3100 to 3000 cm^{-1} [27]. It involves symmetric and

TABLE-4
COMPUTED VIBRATIONAL FREQUENCIES (cm^{-1}) AND ASSIGNMENTS FOR INDOMETACIN IN GASEOUS AND IN DIFFERENT SOLVENTS BASED ON B3LYP/6-31G(d) METHOD

Gas phase	Water (ε = 78.5)	Acetone (ε = 20.493)	Ethanol (ε = 24.852)	Diethyl ether (ε = 4.24)	Vibrational assignments
21.7	21.2	21.7	21.7	21.7	Carboxilic acid group-chlorophenyl ring wagging
24.1	26.3	26.9	26.7	27.4	Carboxilic acid group twisting
29.0	30.4	30.4	30.4	30.4	Carboxilic acid group-indolic, carboxamide ring twisting
31.2	33.2	33.3	33.3	34.1	Carboxilic acid group-indolic, carboxamide ring twisting
51.8	51.0	50.8	50.8	51.0	Chlorophenyl-methoxy wagging
69.8	68.0	68.0	68.0	67.9	Chlorophenyl-methoxy and carboxilic acid group-methyl wagging
74.3	74.7	74.7	74.7	74.0	Chlorophenyl-methoxy and carboxilic acid group-methyl wagging
86.0	83.9	84.1	84.1	85.0	Chlorophenyl-indolic, carboxamide ring wagging
114.0	111.6	111.7	111.7	111.7	Methoxy-methyl twisting
130.2	128.9	129.0	129.0	129.3	Chlorophenyl-indolic, carboxamide ring wagging
142.8	144.6	144.5	144.5	144.3	Methyl rotation
153.7	171.4	171.8	171.6	172.6	Methyl rotation and Indolic-methelene rocking
186.5	185.7	185.9	185.8	185.6	Methyl-methylene rocking
199.1	203.1	203.1	203.1	203.2	Methyl-methylene rocking
210.6	210.4	210.4	210.4	210.8	Chlorophenyl-methoxy rocking
229.6	231.8	232.0	232.0	232.3	Methoxy twisting-chlorophenyl ring distortion
260.8	263.0	263.0	263.0	263.2	Methoxy Twisting-chlorophenyl ring distortion
275.1	273.4	273.5	273.5	273.6	Methoxy Twisting-chlorophenyl ring distortion
278.9	276.2	276.2	276.2	276.3	Methoxy-indolic ring scissoring and chlorophenyl ring distortion
297.7	305.8	305.5	305.6	304.6	Methoxy-indolic ring scissoring and methyl-carboxylic rocking
324.6	323.1	323.1	323.1	323.2	Chlorophenyl scissoring and methyl-carboxylic rocking
340.8	339.7	339.8	339.8	340.2	Methyl-carboxylic oxygen scissoring, indolic and carboxamide rings distortion
361.2	360.2	360.2	360.2	360.3	Indolic ring-methoxy scissoring and metyhlene-methyl scissoring
376.8	375.6	375.8	375.7	376.2	Methyl-methoxy twisting and carboxamide and indolic ring distortion
403.6	402.6	402.8	402.7	402.9	Chlorophenyl, carboxamide and indolic rings distortion
421.5	420.6	420.6	420.6	420.8	Chlorophenyl ring wagging and distortion
431.6	431.4	431.5	431.5	431.9	Chlorophenyl, carboxamide and indolic rings distortion and chlorophenyl ring wagging
448.2	448.3	448.5	448.5	449.0	Indolic, carboxamide and chlorophenyl rings wagging
465.1	459.4	459.6	459.6	460.5	Methyl-methoxy twisting, chlorophenyl, carboxamide and indolic rings distortion
490.5	489.7	489.7	489.7	490.1	Chlorophenyl ring wagging and indolic ring-methoxy scissoring
506.1	505.0	505.1	505.1	505.7	Carboxlic-methelene wagging and carboxamide-indolic ring deformation
527.8	524.1	524.1	524.1	524.4	Indolic-methoxy and methelene-carboxylic rocking
556.3	557.5	557.6	557.5	557.9	Indolic-carboxamide, carboxylic-methyl scissoring and benzoylic ring breathing
598.7	594.9	595.1	595.0	595.8	Indolic-carboxamide scissoring and benzoylic ring breathing
606.3	604.7	604.7	604.7	604.8	Indolic-methoxy, carboxylic scissoring
625.2	625.3	625.4	625.4	625.9	Benzoylic ring, indolic-carboxamide ring rocking and carboxylic scissoring
632.5	632.8	633.0	632.9	633.4	Indolic ring-methoxy rocking and carboxylic out of plane bending
643.3	640.6	640.8	640.8	641.6	Benzoylic and Indolicring Deformation
658.7	654.1	654.7	654.6	656.9	Indolic, carboxamide ring distortion and carboxylic twisting
686.6	662.8	663.6	663.4	668.4	Carboxylic twisting and benzoylic, indolic ring deformation
697.7	691.2	691.3	691.2	691.7	Carboxylic twisting and benzoylic ring deformation
709.6	699.6	699.6	699.6	699.9	Indolic-carboxamide ring distortion and carboxylic twisting
744.8	740.5	740.8	740.7	741.6	Indolic, carboxamide and benzoylic ring distortion
750.8	747.0	747.1	747.1	747.8	Indolic, carboxamide and benzoylic ring distortion
764.2	765.1	765.2	765.1	765.4	Indolic, carboxamide and benzoylic ring distortion
780.7	769.6	769.7	769.7	770.3	Indolic, carboxamide ring deformation and benzoylic wagging
804.7	808.2	808.1	808.1	807.1	Indolic C-H wagging
842.8	843.0	843.0	843.0	843.4	Benzoylic C-H sagging
846.7	849.1	849.2	849.2	849.8	Benzoylic C-H wagging and C (carboxamide) – C (methelene) stretching
860.5	856.9	857.1	857.1	858.1	Benzoylic C-H wagging and indolic C-H twisting
865.0	863.6	863.9	863.8	865.2	Benzoylic C-H wagging and Indolic C-H twisting
887.1	880.1	880.0	880.0	879.8	C (Carboxylic) – C (methelene) stretching and indolic C-H scissoring
919.1	917.6	917.7	917.6	918.0	Methelene rocking and indolic C-H twisting
923.1	931.8	931.2	931.3	928.0	Methelene rocking and indolic C-H twisting
945.7	943.3	943.4	943.4	944.0	Methyl rocking, C (carboxamide) – C (benzoylic) stretching and indolic ring distortion

972.8	976.5	976.3	976.3	975.5	Indolic C-H twisting and methelene C-H rocking
977.9	979.6	979.3	979.4	979.0	Benzoylic C-H twisting
992.0	991.4	991.4	991.5	991.6	Benzoylic C-H twisting, methelene C-H rocking and methyl rocking
1032.4	1028.0	1028.2	1028.1	1029.1	Indolic C-H scissoring, benzoylic scissoring and ring deformation
1039.6	1042.1	1042.3	1042.3	1042.9	Methelene, indolic C-H scissoring and methyl rocking
1074.9	1068.3	1069.1	1069.0	1072.4	Methyl rocking
1079.6	1073.5	1073.8	1073.7	1074.7	Methyl rocking and indolic C-H scissoring
1104.8	1099.7	1100.1	1100.0	1101.7	Methyl rocking, indolic C-H scissoring and benzoylic ring breathing
1109.9	1104.3	1104.5	1104.5	1105.7	Benzoylic ring C-H and methyl scissoring
1141.6	1140.8	1140.7	1140.8	1140.8	Benzoylic ring C-H scissoring
1164.1	1156.6	1156.7	1156.7	1157.1	Benzoylic ring C-H scissoring and methlene C-H twisting
1172.6	1169.8	1169.9	1169.9	1170.4	Indolic C-H scissoring, carboxamide ring distortion and methelene C-H wagging
1184.9	1181.3	1181.2	1181.2	1181.2	Indolic C-H scissoring, carboxamide ring distortion and methelene C-H wagging
1185.7	1182.5	1182.6	1182.6	1183.2	Methoxy rocking
1211.8	1207.8	1207.9	1207.9	1208.7	Chlorophenyl C-H scissoring
1217.7	1214.3	1214.5	1214.5	1215.2	Methoxy C-H rocking and indolic ring breathing
1230.5	1227.6	1227.7	1227.7	1228.2	Carboxamide ring breathing, indolic C-H scissoring, methylene twisting and carboxylic acid group deformation
1252.8	1251.5	1251.7	1251.7	1252.6	Chlorophenyl ring breathing, indolic C-H twisting, indolic oxygen-methoxy carbon stretching and C (carboxamide) – C (chlorophenyl) stretching
1269.9	1269.8	1270.0	1270.0	1270.8	Methylene twisting, carboxamide symmetrical stretching and indolic C-H wagging
1284.9	1281.9	1282.1	1282.0	1282.9	Chlorophenyl, indolic and carboxamide rings deformation
1318.2	1315.8	1315.8	1315.8	1316.1	Methylene C-H rocking, carboxylic acid group scissoring and indolic ring breathing
1327.5	1326.6	1326.7	1326.7	1327.2	Indolic C-H rocking and ring deformation
1334.2	1334.3	1334.1	1334.2	1333.9	Chlorophenyl C-H rocking and ring deformation
1344.5	1342.1	1342.3	1342.3	1343.1	Chlorophenyl ring deformation
1358.4	1349.9	1350.5	1350.3	1352.9	Indole, carboxamide, chlorophenyl rings deformation and N-C stretching
1388.6	1390.0	1390.0	1390.0	1389.9	Indole, carboxamide rings deformation, carboxylic scissoring and methyl scissoring
1406.7	1404.8	1405.1	1405.0	1406.0	Indole, carboxamide rings deformation and carboxylic scissoring
1423.2	1415.3	1415.4	1415.4	1416.0	Indole, carboxamide rings deformation and carboxylic scissoring
1443.1	1440.2	1440.3	1440.3	1441.0	Chlorophenyl C-H scissoring
1452.8	1447.1	1447.5	1447.4	1449.2	Methyl C-H wagging
1486.7	1475.2	1475.6	1475.5	1477.8	Indole, carboxamide rings deformation, methylene and methyl C-H scissoring
1494.3	1490.5	1490.8	1490.7	1491.9	Indole, carboxamide rings deformation, methylene and methyl C-H scissoring
1499.2	1495.1	1495.7	1495.6	1497.9	Methylene and methyl C-H scissoring
1503.4	1497.7	1498.0	1498.0	1499.4	Indole, carboxamide rings deformation, methylene and methyl C-H scissoring
1514.3	1507.9	1508.4	1508.3	1510.6	Methylene and methyl C-H scissoring, in-plane bending
1521.9	1513.9	1514.4	1514.3	1516.5	Methoxy C-H scissoring
1526.0	1520.2	1520.6	1520.5	1522.4	Indole, carboxamide rings deformation and methoxy scissoring
1534.8	1531.7	1531.9	1531.9	1532.8	Chlorophenyl ring deformation and rocking
1539.5	1532.6	1532.9	1532.8	1534.6	Methoxy C-H scissoring
1620.6	1619.5	1619.6	1619.5	1619.9	Chlorophenyl ring deformation
1626.6	1624.1	1624.4	1624.4	1625.7	Indole and carboxamide rings deformation
1647.6	1642.3	1642.6	1642.5	1643.9	Chlorophenyl ring deformation
1659.4	1658.6	1659.1	1659.0	1660.9	Indole and carboxamide rings deformation
1677.6	1673.0	1673.4	1673.3	1675.1	Indole, carboxamide rings deformation and C=O stretching
1759.1	1734.8	1736.2	1735.9	1742.7	C=O stretching
1850.1	1820.1	1822.5	1822.0	1832.7	Carboxylic C=O stretching
3021.8	3035.9	3034.9	3035.1	3030.8	Methoxy C-H symmetric stretching
3050.5	3057.4	3057.6	3057.5	3057.9	Methlene C-H symmetric stretching
3070.5	3067.6	3067.7	3067.6	3067.7	Methyl C-H symmetric stretching
3079.1	3097.7	3096.4	3096.7	3091.2	Methoxy C-H asymmetric stretching
3113.6	3102.7	3101.9	3102.1	3098.8	Methlene C-H asymmetric stretching
3126.9	3126.1	3126.2	3126.2	3126.5	Methyl C-H asymmetric stretching
3154.3	3153.7	3153.5	3153.5	3152.6	Methoxy C-H asymmetric stretching
3157.4	3162.3	3161.9	3161.9	3159.9	Methyl C-H asymmetric stretching
3210.0	3209.6	3210.0	3209.9	3211.1	Indolic C-H stretching

3218.8	3222.8	3222.5	3222.6	3221.5	Chlorophenyl C-H asymmetric stretching
3220.3	3223.9	3223.7	3223.7	3222.7	Chlorophenyl C-H asymmetric stretching
3227.5	3234.1	3233.5	3233.6	3231.3	Indolic C-H asymmetric stretching
3232.2	3235.9	3235.6	3235.7	3234.5	Chlorophenyl C-H asymmetric stretching
3233.4	3237.3	3237.0	3237.1	3235.9	Chlorophenyl C-H symmetric stretching
3243.2	3247.6	3247.2	3247.3	3245.8	Indolic C-H symmetric stretching
3681.5	3678.5	3678.9	3678.8	3681.3	Carboxylic O-H stretching

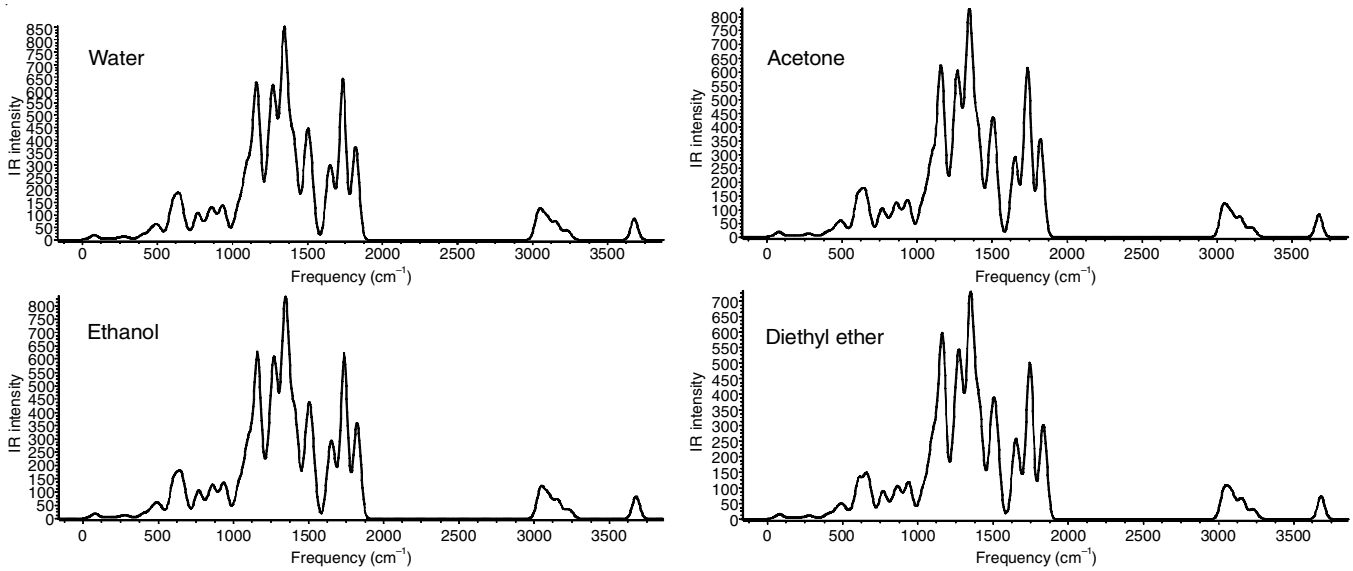

Fig. 5. Recorded IR intensities of indometacin in different solvents

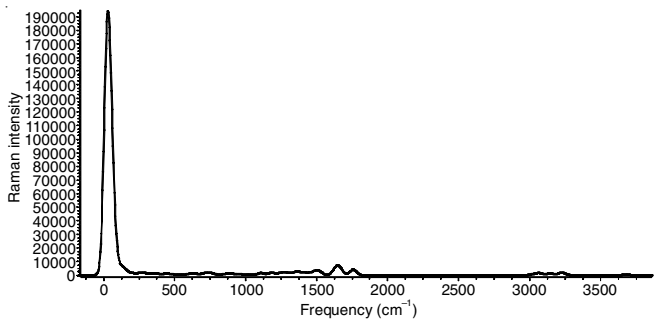

Fig. 6. Recorded Raman intensities of indometacin in the gas phase

asymmetric C-H stretching associated with its methyl, methylene, methoxy groups, chlorophenyl and indolic ring C-H bonds. The aqueous environment slightly influences the spectral intensities of indometacin. These C-H stretching vibrations in water are observed between 3248 and 3035 cm^{-1}. Almost similar values are noted for indometacin in acetone and ethanol. At the same time, the C-H vibrations are recorded from 3246 to 3031 cm^{-1} for the title molecule in diethyl ether involving the same chemical groups as that of other compounds. Generally, the vibrational frequencies ranging from 1650 and 1400 cm^{-1} are assigned to the C-C stretching vibrations in the compounds

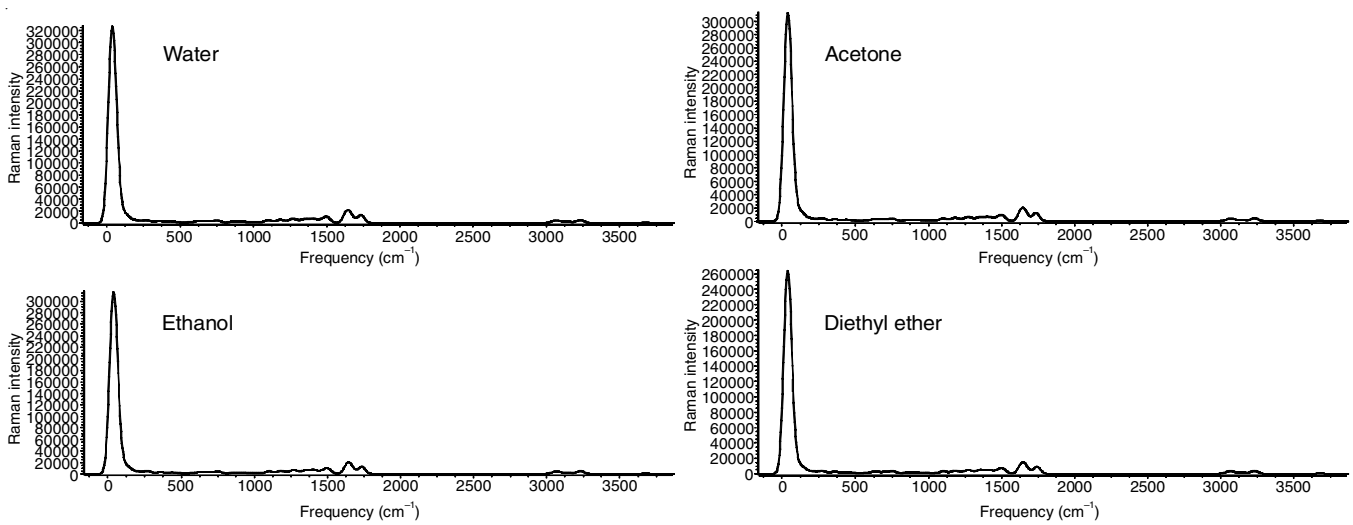

Fig. 7. Recorded Raman intensities of indometacin in different solvents

involving benzene rings [28]. For indometacin, in gaseous and aqueous phases, the carboxamide, indole and chlorophenyl rings invol-ving C-C bonds experience deformations due to C-C stretching predominantly between 1677-1406 cm^{-1}. These ring deforma-tions have been observed in the range of 1673-1404 cm^{-1} for the title molecule in water and 1673-1405 cm^{-1} in acetone and ethanol. In diethyl ether, the C-C stretching and ring deformations are recorded between 1675 and 1406 cm^{-1}.

Indometacin possesses methoxy and methylene groups (Fig. 1). For the methylene group frequency assignments, essentially, nine modes are considered *viz.* symmetric and asymmetric stretching, scissoring (in and out-of-plane), in-plane and out-of-plane bending, twisting (in-plane and out-of-plane) and torsional mode [29]. Usually, methyl in-plane bending takes place around 1518 and 1450 cm^{-1} and strictly at 1514 cm^{-1}. In present work, indometacin accurately exhibits the methylene in plane bending (scissoring) at 1514 cm^{-1} in gas phase, which is very well supported by previous studies [29]. The same has been observed at 1507, 1508 and 1510 cm^{-1} in IM-W, IM-A and IM-E, IM-D, respectively. The indometacin methoxy C-H scissoring is exhibited at 1522 cm^{-1} in the gas phase. In aqueous phases, interestingly, this happens at the frequency predicted for methylene scissoring (around 1514 cm^{-1}). The methyl twisting in gas phase indometacin is detected at 465 cm^{-1}, which are found to be comparable with traditional computational values (464 and 470 cm^{-1}) [29]. The aqueous surroundings have a notable influence on this phenomenon and it is observed at 460 cm^{-1} almost in all the solvents, irrespective of their dielectric constants. The methylene C-H wagging is mainly observed at 1172 and 1185 cm^{-1}.

The C=O stretching is observed at 1759 cm^{-1} (C5-O11) (Fig. 1) and 1850 cm^{-1} in the carboxylic group of indometacin. This has been observed at considerably lower frequencies in solution phases (Table-4). The carboxylic C=O out-of-plane bending is computed at 632 cm^{-1} for indometacin in the gas phase and there is not much variation in its solution phases. The C-N stretching vibration of indometacin is recorded at 1358 and 1344 cm^{-1} in gas; around 1350 and 1342 cm^{-1} in aqueous phases, which is well supported by the standard values (1300 cm^{-1}) reported in previous study [30]. The frequency of C-Cl stretching is usually present between 800-600 cm^{-1} based on the molecular configuration [31]. Here, the benzoylic ring (involving C-Cl bond) disturbances in terms of breathing, scissoring and distortions begin at 598 cm^{-1} and extend till 865 cm^{-1} for indometacin. The C-Cl stretching explicitly occurs at 751 and 745 cm^{-1}, which leads to benzoylic ring distortion of indometacin in its gas phase and it was observed at around 781 and 740 cm^{-1} in its aqueous environments. The vibrations involving rings are not pure and considerably affected by other vibrations and the substituents added. In indometacin, ring in-plane and out-of-plane bending modes are observed mainly from 448 to 230 cm^{-1} involving chlorophenyl, indolic, carboxamide ring wagging, twisting, scissoring and ring deformations. The bands obtained from 973 cm^{-1} onwards, the C-H rocking are measured in CH_3 in-plane and out-of-plane modes. Specifically, 1105 cm^{-1} is characterised to the benzoylic ring breathing in the title molecule, followed by its benzoylic ring scissoring at 1110 and 1142 cm^{-1}.

The translational, rotational and vibrational thermal energies, specific heat, entropy, zeropoint vibrational energy (ZPVE) and rotational constants of indometacin in gas and solution phases, which have been obtained in the ground state are presented in Table-3. The ZPVE of indometacin in the gas phase is found to be 197.731 Kcal/mol. Out of the solvated indometacin complexes, the minimum ZPVE is observed for IM-W and the maximum is for IM-D and the order based on ZPVE provides strong support for the stability order anticipated by the relative energies. The computed vibrational and thermal energies also follow a similar trend. The calculated rotational constants of indometacin in aqueous phases (Table-3) show that the different aqueous environments do not impact them much. The calculated entropy values of solvated indometacin are IM-W > IM-E > IM-A > IM-D.

Highest occupied molecular orbitals (HOMO) describes the ability of electron donation and it is known to be an electron donor region and measures the ionization potentials. Lowest unoccupied molecular orbital (LUMO) symbolizes the electron acceptor regions that determine the electron affinity and the capability to get an electron. The higher values of HOMO show the more significant electron-donating ability of the complexes. The lower LUMO values indicate the ability of electron acceptance. The nature of the HOMO-LUMO plot for the most stable aqueous phase structure IM-W is shown in Fig. 8. The HOMO is located at the indole ring of indometacin, with the most negli-

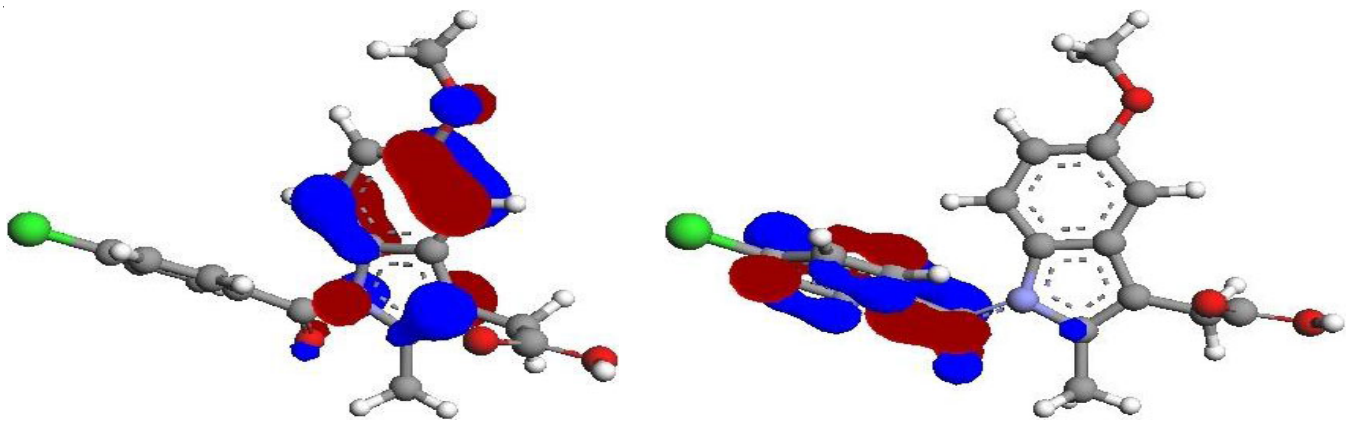

Fig. 8. Molecular orbitals for the HOMO and LUMO of indometacin in the most stable aqueous phase (water)

gible contribution from the five-membered ring with nitrogen. The LUMO is localized on the chlorophenyl group of indometacin.

The molecular electrostatic potential (MEP) map is a tool for the prediction and representation of the chemical and molecular reactive characteristics of the molecule. The 3D illustration of the distribution of charges of molecules and it helps to understand the differently charged regions present in a molecule [32]. The MEP map symbolizes the electron wealthy and poor regions by red and blue colours, respectively. The zero electrostatic potential areas are represented by green. In most MEP surfaces, the electrophilic attack occurs at negative (electron rich) regions, and the nucleophilic attack occurs at positive (electron-poor) regions. Out of all the aqueous phases, indometacin is found to be stable in water and its MEP map is presented in Fig. 9. Here, the red colour is concentrated at oxygen atoms of indomethacin (O11, O23 and O32) of indometacin, which qualifies it as an electron-rich region favourable for the electrophilic interaction and the blue is located near the chlorine atom of indometacin, which makes it suitable for nucleophilic attack.

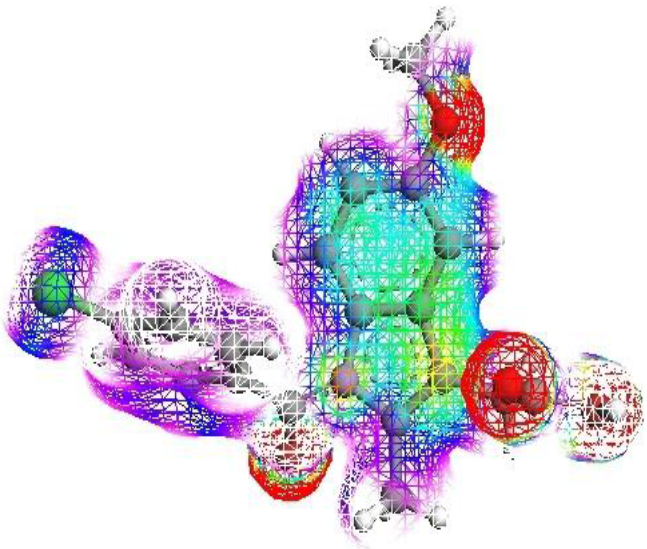

Fig. 9. Molecular electrostatic potential (MEP) mapping of indometacin in the most stable aqueous phase (water)

Conclusion

In this study, the solubility of indometacin has been studied in various solution phases through the B3LYP/6-31G(d) level of theory. The stability order is IM-W > IM-E > IM-A > IM-D. It has been observed that the stability of solvated indometacin increases with increasing dielectric constants as well as the dipole moments. The IR and Raman vibrational assignments of indometacin have been explored theoretically with DFT/B3LYP method by employing the same basis set and are found to agree with the prescribed values. The dipole moment, thermo dynamical parameters, and rotational constants were determined from the DFT calculations. The HOMO-LUMO of the title molecule was investigated and exhibited the electron donor and acceptor regions of indometacin. The MEP mapping predicted the reactive molecular characteristics of the indometacin.

CONFLICT OF INTEREST

The authors declare that there is no conflict of interests regarding the publication of this article.

REFERENCES

1. A. Dandic, K. Rajkovaca, M. Jozanovic, I. Pukleš, A. Széchenyi, M. Budetic and M. Samardzic, *Rev. Anal. Chem.*, **41**, 34 (2022); https://doi.org/10.1515/revac-2022-0032
2. S. Nalamachu and R. Wortmann, *Postgrad. Med.*, **126**, 92 (2014); https://doi.org/10.3810/pgm.2014.07.2787
3. M.D. Villar-Martínez, D. Moreno-Ajona MD, C. Chan and P.J. Goadsby, *Headache*, **61**, 700 (2021); https://doi.org/10.1111/head.14111
4. L.C. Sowers, L.S. Blanton, S.C. Weaver, R.J. Urban and C.P. Mouton, *J. Transl. Sci*., **6**, 394 (2020).
5. F. Shakeel, F.K. Alanazi, I.A. Alsarra and N. Haq, *J. Mol. Liq*., **188**, 28 (2013); https://doi.org/10.1016/j.molliq.2013.09.013
6. L. Xu, Y. Li, P. Jing, G. Xu, Q. Zhou, Y. Cai and X. Deng, *Spectrochim. Acta A Mol. Biomol. Spectrosc.*, **249**, 119309 (2021); https://doi.org/10.1016/j.saa.2020.119309
7. B. Rossi, P. Verrocchio, G. Viliani, G. Scarduelli, G. Guella and I. Mancini, *J. Chem. Phys.*, **125**, 044511 (2006); https://doi.org/10.1063/1.2217952
8. A. Parkan, M. Mirzaei, N. Tavakoli and A. Homayouni, *Main Group Chem.*, **21**, 611 (2022); https://doi.org/10.3233/MGC-210157
9. M.S. Alsalhi and K.L. Andrew Chan, *Int. J. Pharm*., **617**, 121591 (2022); https://doi.org/10.1016/j.ijpharm.2022.121591
10. M.S. Alsalhi and K.L.A. Chan, *Int. J. Pharm.*, **617**, 121591 (2022); https://doi.org/10.1016/j.ijpharm.2022.121591
11. A.K. Jain, *Eur. J. Pharm. Biopharm.*, **68**, 701 (2008); https://doi.org/10.1016/j.ejpb.2007.06.013
12. X. Qi, J. Zhang, W. Wang and D. Cao, *Pharm. Dev. Technol.*, **18**, 852 (2013); https://doi.org/10.3109/10837450.2011.595797
13. E.I. Yackevich, A.B. Mirgorodskaya, L.Y. Zakharova and O.G. Sinyashin, *Russ. Chem. Bull.*, **64**, 2232 (2015); https://doi.org/10.1007/s11172-015-1143-8
14. S. Kulkarni, S.P. Gupta, N. Upmanyu and S.D. Tonpay, *J. Chem. Pharm. Res.*, **3**, 280 (2011).
15. P.K. Shende, R.S. Gaud, F. Naik and A. Deshmukhe, *J. Anal. Pharm. Res.*, **3**, 1 (2016); https://doi.org/10.15406/japlr.2016.03.00079
16. N. Rodríguez-Laguna, L.I. Reyes-García, R. Moya-Hernández, A. Rojas-Hernández and R. Gómez-Balderas, *J. Chem.*, **24**, 9804162 (2016); https://doi.org/10.1155/2016/9804162
17. Y. Wang, E. Bolton, S. Dracheva, K. Karapetyan, B.A. Shoemaker, T.O. Suzek, J. Wang, J. Xiao, J. Zhang and S.H. Bryant, *Nucleic Acids Res.*, **38(S1)**, D255 (2010); https://doi.org/10.1093/nar/gkp965
18. C. Lee, W. Yang and R.G. Parr, *Phys. Rev. B Condens. Matter*, **37**, 785 (1988); https://doi.org/10.1103/PhysRevB.37.785
19. J.P. Perdew and Y. Wang, *Phys. Rev. B Condens. Matter*, **45**, 13244 (1992); https://doi.org/10.1103/PhysRevB.45.13244
20. M.J. Frisch, G.W. Trucks, H.B. Schlegel, G.E. Scuseria, M.A. Robb, J.R. Cheeseman, G. Scalmani, V. Barone, B. Mennucci, G.A. Petersson, H. Nakatsuji, M. Caricato, X. Li, H.P. Hratchian, A.F. Izmaylov, J. Bloino, G. Zheng, J.L. Sonnenberg, M. Hada, M. Ehara, K. Toyota, R. Fukuda, J. Hasegawa, M. Ishida, T. Nakajima, Y. Honda, O. Kitao, H. Nakai, T. Vreven, J.A. Montgomery, Jr., J.E. Peralta, F. Ogliaro, M. Bearpark, J.J. Heyd, E. Brothers, K.N. Kudin, V.N. Staroverov, T. Keith, R. Kobayashi, J. Normand, K. Raghavachari, A. Rendell, J.C. Burant, S.S. Iyengar, J. Tomasi, M. Cossi, N. Rega, J.M. Millam, M. Klene, J.E. Knox, J.B. Cross, V. Bakken, J. Jaramillo, R. Gomperts, R.E. Stratmann, O. Yazyev, C. Adamo, A.J. Austin, R. Cammi, C. Pomelli, J.W. Ochterski, R.L. Martin, K. Morokuma, V.G. Zakrzewski, G.A. Voth, P. Salvador,

J.J. Dannenberg, S. Dapprich, A.D. Daniels, O. Farkas, J.B. Foresman, J.V. Ortiz, J. Cioslowski,and D.J. Fox, Gaussian, Inc., Wallingford CT, Gaussian 09, revision B.01 (2010).
21. A. Frisch, A.B. Nielsen and A.J. Holder, Gauss View, Gaussian Inc. (2000).
22. S. Miertus and J. Tomasi, *Chem. Phys.*, **65**, 239 (1982); https://doi.org/10.1016/0301-0104(82)85072-6
23. S.P. Singh, C.R. Deb, S.U. Ahmed, Y.S. Chandra and B.K. Konwar, *J. Bio. Nanosci.*, **8**, 328 (2014).
24. R. Karunathan, V. Kannappan and V. Sathyanarayanamoorthi, *Elixir Computat. Chem.*, **71**, 24793 (2014).
25. P. Anbarasu, M. Arivazhagan and V. Balachandran, *Indian J. Pure Appl. Phys.*, **50**, 91 (2012).
26. L. Dan, G.-M. Zhou, L.-T. Zhang and C.-H. Zhang, *Spectrosc. Spectr. Anal.*, **38**, 3112 (2018); https://doi.org/10.3964/j.issn.1000-0593(2018)10-3112-05
27. M. Saranya, S. Ayyappan, R. Nithya, A. Gokila and R.K. Sangeetha, *Dig. J. Nanomater. Biostruct.*, **12**, 127 (2017).
28. G. Ilango, M. Arivazhagan, J. Joseph Prince and V. Balachandran, *Indian J. Pure Appl. Phys.*, **46**, 698 (2008).
29. A. Thirunavukkarasu, R. Karunathan, V. Sathyanarayanamoorthi and J. Mallika, *Indian J. Pure Appl. Phys.*, **52**, 653 (2014).
30. N.P.G. Roeges, A Guide to the Complete Interpretation of Infrared Spectra of Organic Structures, Wiley: New York (1994).
31. V. Krishnakumar, S. Dheivamalar, R.J. Xavier and V. Balachandran, *Spectrochim. Acta A Mol. Biomol. Spectrosc.*, **65**, 147 (2006); https://doi.org/10.1016/j.saa.2005.09.039
32. R.K. Sangeetha and S. Ayyappan, *Dig. J. Nanomater. Biostruct.*, **15**, 123 (2020); https://doi.org/10.15251/DJNB.2020.151.123